A thermogravimetric comparative study of the high temperature steam oxidation of bare and pre-oxidized Zircaloy-4, M5Framatome and Optimized ZIRLO™

Christian Duriez, H. Richez, C. Eymery, J. Desquines, Severine Guilbert

Journal of Nuclear Materials 597 (2024) 155147

Contents lists available at ScienceDirect

Journal of Nuclear Materials

journal homepage: www.elsevier.com/locate/jnucmat

A thermogravimetric comparative study of the high temperature steam oxidation of bare and pre-oxidized Zircaloy-4, $M5_{Framatome}$ and Optimized ZIRLO™

C. Duriez [a,*], H. Richez [b], C. Eymery [c], J. Desquines [a], S. Guilbert [a]

[a] Institut de Radioprotection et de Sûreté Nucléaire (IRSN), PSN-RES, Cadarache BP 3, 13 115 St Paul-Lez-Durance cedex, France
[b] Institut National des Sciences Appliquées (INSA) – Université de Rennes 1, Rennes, France
[c] Aix-Marseille Université, Marseille, France

ARTICLE INFO

Keywords:
M5
Optimized-ZIRLO
LOCA
High temperature oxidation
Thermogravimetry

ABSTRACT

For Loss of Coolant Accident (LOCA) analysis, high-temperature oxidation kinetics in steam of Zircaloy-4 and the two Nb-bearing alloys used in French Pressurized Water Reactors (PWRs), $M5_{Framatome}$[1] and Optimized ZIRLO™[2], have been studied using Thermo-Gravimetric Analysis (TGA) technique in the temperature range of 900–1200 °C. A specific test procedure allowing the use of a high steam flow rate and good steam supply to the whole specimen surface, as well as fast heating of the specimen, has been developed. Clean kinetic data, not affected by steam starvation, were obtained on the bare, as-received alloys. For as-received claddings, oxidation kinetics are comparable and close to parabolic for the three alloys at 1100 °C and above. Below 1100 °C, a significant deviation from the parabolic kinetic regime was observed, and $M5_{Framatome}$ oxidizes slower than Zircaloy-4 and Optimized ZIRLO. Thanks to the fast-heating protocol, the influence of pre-oxidation, simulating corrosion in normal reactor operation, could be investigated, avoiding evolution of the pre-oxidation scale during a slow, long heating phase. Pre-oxidized Zircaloy-4 and $M5_{Framatome}$ were investigated. A strong protective effect is observed below 1200 °C, while at 1200 °C, the pre-oxidation layer appears to be much less protective, possibly due to the monoclinic to tetragonal zirconia phase transformation.

1. Introduction

In a Loss Of Coolant Accident (LOCA), the exothermic oxidation of the cladding material in high-temperature steam contributes to temperature escalation, and is accompanied by the release of massive amounts of gaseous hydrogen, which is a critical safety concern. The oxidation reaction also weakens the cladding and can result in rod rupture, extensive fuel dispersal, and ultimately, the loss of coolable geometry. The high-temperature oxidation kinetics of Zirconium (Zr) alloys have been studied since the 1950s, initially focusing on the Zircaloys class of alloys. Oxidation tests were initially conducted using as-received materials, and the acceptance criteria for Emergency Core Cooling Systems (ECCS) in 1973 [1] were based on oxidation measurement campaigns using fresh Zircaloy-4 (the historical Zr-alloy for Pressurized Water Reactors, PWR). For a comprehensive review of these experimental data, refer to Hache and Chung [2]. Subsequently, the influence of zirconia corrosion scale formation on the claddings during normal operation has been considered, either by utilizing laboratory-prepared pre-oxidized specimens [3-8] or [3-8] or with irradiated defueled rods [9-12].

Most high-temperature oxidation tests on Zirconium alloys are isothermal interrupted tests, wherein the weight gain, attributed solely to oxygen uptake, is determined by weighing the specimen before and after a specified exposure duration. Consequently, a relatively large number of tests are required to establish a complete kinetic curve. For well-controlled isothermal conditions, both the heating and cool-down

* Corresponding author.
E-mail address: christian.duriez@irsn.fr (C. Duriez).

[1] M5 and $M5_{Framatome}$ are trademarks or registered trademarks of Framatome or its affiliates, in the USA or other countries.

[2] Optimized ZIRLO is a trademark or registered trademark of Westinghouse Electric Company LLC, its affiliates and/or its subsidiaries in the United States and may be registered in other countries throughout the world. All rights reserved. Unauthorized use is strictly prohibited. Other names may be trademarks of their respective owners.

https://doi.org/10.1016/j.jnucmat.2024.155147
Received 29 February 2024; Received in revised form 26 April 2024; Accepted 30 April 2024
Available online 4 May 2024

rates should be high. To achieve this, heating systems with low thermal inertia have often been utilized, including laser heating [13], infrared lamp furnaces [9-12], and electromagnetic induction heating [3,14]. However, resistive furnaces offer easier temperature control and better homogeneity. To facilitate rapid heating, the specimen can be initially kept in a cold zone while the furnace is heated, then inserted into the hot zone for a specified duration, and finally removed from the hot zone for rapid cooldown. This procedure has been employed in numerous laboratories [3,7,8,14-17]. For even faster cooldown, the specimen may be quenched in water after extraction [7,8,15,16]. The heating and cooldown rates achieved with this protocol typically reach around 100 °C/s.

An appealing alternative to the interrupted test protocol is the Thermogravimetric Analysis (TGA) technique, which allows for online measurement of the specimen's weight change during its reaction. A complete oxidation curve is obtained within a single experiment, and the reaction rate can be straightforwardly derived by the time derivation of the weight increase signal, enabling analysis in terms of oxidation regimes. TGA has been utilized at IRSN and other laboratories for cladding oxidation studies related to Spent Fuel Pool LOCA (SFP-LOCA) [18-23], for which the temperature domain of interest is somewhat lower than for core large break LOCA. One limitation of the TGA technique is its low heating rate, typically a few tens of degrees Celsius per minute for commercial, resistive furnace-based apparatus. For isothermal tests, the reactive gas must be injected after a heating phase under an inert atmosphere. In high-temperature oxidation tests, there is a concern regarding possible alteration of the specimen during the slow and rather long (compared to the oxidation duration) heating phase. Specifically, with pre-oxidized cladding specimens, at least partial dissolution of the low-temperature zirconia scale may occur during heat-up. A second limitation of commercial TGA instruments is the low permissible gas flow rates. This can be a significant drawback for LOCA studies, given the high oxidation rates of zirconium alloys at high temperature [18,24]. This is likely the main reason why this technique has been scarcely used in this domain. Nevertheless, a few rather recent oxidation studies covering the temperature range of interest for in-reactor large break LOCA using the TGA technique have been published [25-31]. In Refs. [28,29] and [30], however, the steam flow rates used are low, and steam starvation conditions have to be suspected, as revealed in [28] and [29] by the high hydrogen concentrations incorporated in the metal during the oxidation tests, conditions where they were not expected (away from the breakaway domain). The use of a low steam flow rate can have a significant impact on the oxidation process and its kinetics, as will be discussed in the present paper.

For the present study, sets of TGA steam oxidation tests were conducted on Zircaloy-4, $M5_{FRAMATOME}$, and Optimized ZIRLO alloys (referred to as Zy4, M5, and OZ respectively) in the temperature range of 900–1200 °C. A commercial SETARAM thermobalance was modified to accommodate high steam flow rates, and a specific test protocol was employed to achieve rapid heating and cooling rates. Comparisons were made between the three alloys and results obtained from interrupted tests. Subsequently, the influence of a low-temperature pre-oxidation layer simulating in-reactor corrosion was evaluated and discussed.

2. Experimental

2.1. Material

For each batch, 20 mm long tube specimens were cut from 17×17 PWR cladding tubes. The Zircaloy-4 Stress Relieved Annealed (SRA) tubes were provided by AREVA (now Framatome). For M5, two batches were used, provided by Framatome. The Optimized-ZIRLO batch was provided by Westinghouse. Both the M5 and OZ alloys were recrystallized (RXA). Zy4 and M5 batch 1 were used for both as-received and pre-oxidized specimens, M5 batch 2 for pre-oxidized specimens only, and OZ for as-received specimens only. Chemical composition of the ingots, as provided by the manufacturers, is presented in Table 1.

2.2. Pre-oxidation

The objective of pre-oxidation is to form a zirconia layer on the cladding surface that simulates, as closely as possible, the waterside corrosion layer that develops on the cladding's outer surface during normal in-reactor operation. Similar to previous studies [7,32], cladding specimens were pre-oxidized in a resistive furnace at 425 °C in a flowing O_2 + steam mixture. Depending on the alloy, the steam partial pressure was adjusted to achieve similar amounts of hydrogen incorporation in the metal as those measured after waterside corrosion in PWRs. Table 2 provides the pre-oxidation conditions and main features of the different pre-oxidized batches prepared for this study, including steam partial pressures of the furnace atmosphere, pre-oxidation durations, mean zirconia scale thicknesses (calculated from the weight gain assuming 97 % dense zirconia on one side, and measured by optical microscopy on polished radial cross-sections when available on the other side), growth rates, hydrogen contents measured by hot extraction with a LECO instrument, and equivalent Hydrogen Pick-Up Fraction (HPUF). This parameter is calculated assuming that only steam contributes to the oxidation. While this assumption is not entirely accurate, the HPUF parameter serves as a measure of the amount of hydrogen incorporated per amount of ZrO2 formed, providing a comparison point with the HPUF observed for in-reactor corrosion (17–18 % for Zy4, 7–10 % for [33]). It is important to note that because our pre-oxidations are double-sided, a given HPUF will result in a two-fold increase in hydrogen incorporation compared to single-side corrosion. For M5, a first series was produced under 150 hPa steam partial pressure, resulting in excessive hydrogen incorporation. For the second series, the steam partial pressure was lowered to 12 hPa, leading to hydrogen amounts closer to expectations. However, for two batches of this second series, the hydrogen amounts incorporated were too high, likely due to malfunctioning of the steam flow controller. Fig. 1 shows examples of cross-sections of pre-oxide scales grown on Zy4 and M5 cladding substrates. In these examples, the scale thickness was 32 μm for Zy4 and 20 μm for M5. While the samples were double-sided oxidized, only the outer oxide scales are displayed in Fig. 1. The inner scale thickness was observed to be about 10–15 % lower than the outer scale thickness, for both Zy4 and M5. The values given in the 6th column of Table 2 are mean values over the inner and outer thicknesses.

Table 1
Ingots mass composition (data from vendors).

	Fab. year	Nb (%)	Sn (%)	Fe (ppm)	Cr (ppm)	O (%)	C (ppm)	Si (ppm)	S (ppm)	H (ppm)
Zy4 SRA	2000	<0.004	1.29–1.31	2100–2200	1100	0.127–0.137	149–163	89–94	13–23	≤ 3
M5 batch 1	2004	0.99–1.01	< 0.003	303–328	41–44	0.139–0.149	22.26	<10	14–18	≤ 3
M5 batch 2	2019	0.97–1.00	< 0.0025	345–390	< 50	0.130–0.140	70–80	<10	14–23	≤ 4
OZ	2021	0.9–1.0	0.65–0.70	1000–12,000	56–69	0.113–0.124	<60	43–50	<25	<10

2.3. TGA apparatus

A SETARAM SETSYS single-furnace thermobalance was utilized for the high-temperature steam oxidation tests. A mixture of steam and argon was injected from the bottom of the furnace, while a helium counterflow protected the balance measurement head from steam condensation. The steam flow rate was adjusted within the range of 14.5–100 g/h (see Section 2.4), and the argon flow rate was adapted accordingly to maintain a 30 % steam volume fraction, the maximum fraction allowed with the SETARAM instrument to prevent condensation in the reactive gas injection circuit. For instance, the argon flow rate was set to 0.7 Nl/min for a steam flow rate of 14.5 g/h. Steam flow rates mentioned later in this document, given in g/h, always refer to steam only. A type B thermocouple was point-welded onto each specimen for temperature measurement. Additionally, it served as a convenient suspension device, eliminating the need for drilling holes in the tubes, while minimizing perturbations to the steam flow on both the inner and outer surfaces. Different configurations were employed, as illustrated in Fig. 2: for as-received specimens, the thermocouple wires were welded onto the lateral external face (Fig. 2a). For pre-oxidized specimens, the thermocouple wires were welded onto the upper end section, either at two different points (Fig. 2b) or at a single point (Fig. 2c). The welding technique employed, spot arc welding, delivers a limited amount of energy, and the volume where microstructural changes occur is small. Based on a metallographic cross-section of the weld, it has been estimated that the diameter of the heat affected zone is about 400 μm and that the fraction of the surface affected by the welding is approximately 0.007 % of the total surface exposed to oxidation. Consequently, the influence on the mass gain is negligible.

Because the SETARAM furnace can achieve only moderate heating rates, not exceeding a few tens of degrees Celsius per minute, the following test procedure was employed: while the furnace was left open and the specimen was maintained outside, the argon flow was initiated, and the furnace was heated. Subsequently, the steam flow was initiated. After the furnace reached the desired temperature plateau and the temperature was stabilized, the specimen was lowered into the hot zone at a constant speed of 1 cm/s. The heat released by oxidation contributed to the specimen's temperature rise, and this contribution became particularly significant at high temperatures for as-received specimens due to the rapid oxidation of the bare metal. Indeed, the rate of temperature rise of the specimen, as directly measured by the thermocouple welded onto the cladding tube, was observed to depend on the furnace temperature as well as the initial state of the specimen, whether it was as-received or pre-oxidized. This rate varied between 15 and 100 °C/s (see Table 3), values far above the heating rates typically attainable with conventional use of the SETARAM instrument. Therefore, this procedure

Table 2
Main characteristics of pre-oxidized cladding batches.

	P_{H2O} (hPa)	Duration (day)	Mean pre-ox scale thickness from mass gain (μm)	Growth rate (μm/day)	Mean pre-ox scale thickness from metallography	H content (wppm)	HPUF (%)
Zy4	150	256	26.5 - 32	0.1 – 0.125	26–35	300 - 360	8 - 9
$M5_{Framatome}$ 1st series	150	258	18 - 23	0.07 – 0.09		200 - 250	10 - 12
$M5_{Framatome}$ 2nd series	12	47	5.03	0.18	4.7 ± 1	30	4.2
	12	117	13.7	0.12	12.15 ± 1	45	2.3
	?	147	8.9	0.06	8.9 ± 1.1	80	7.2
	12	167	20.9	0.125	19.2 ± 2.0	50	1.8
	?	172	21.5	0.125	19.5 ± 1.3	170	7.2

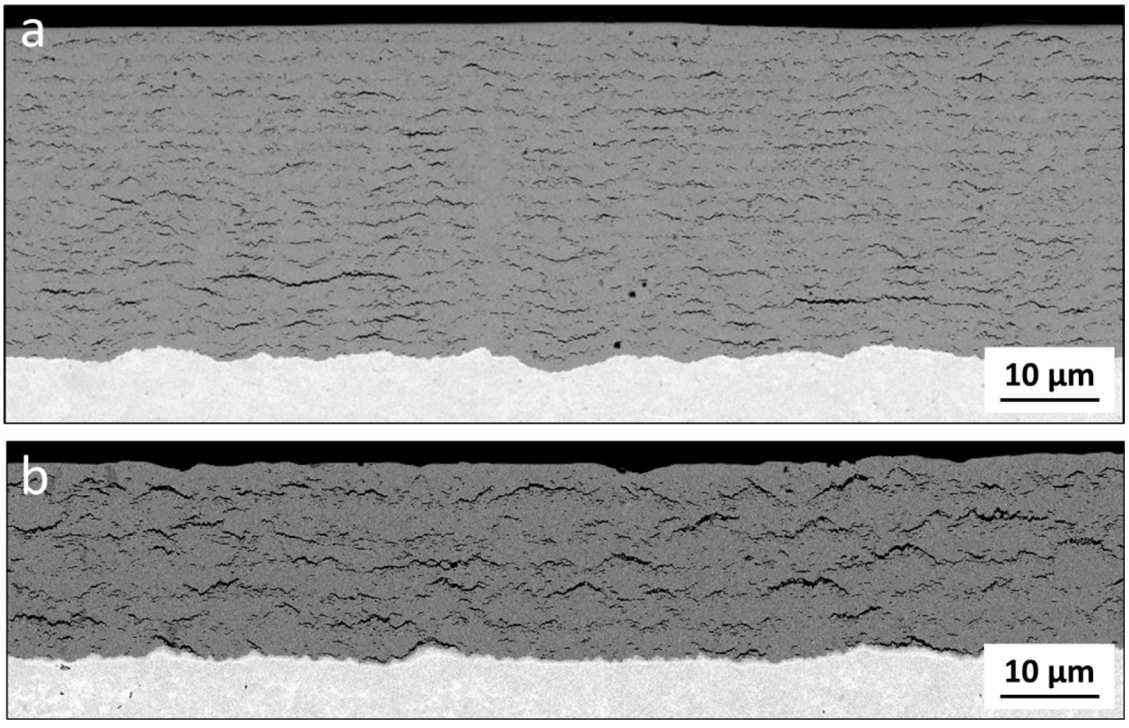

Fig. 1. Secondary Electron Microscopy (SEM) cross sections of pre-oxide scales grown at 425 °C in $O_2 + H_2O$. a. Zy4, 256 days; b. M5, 167 days.

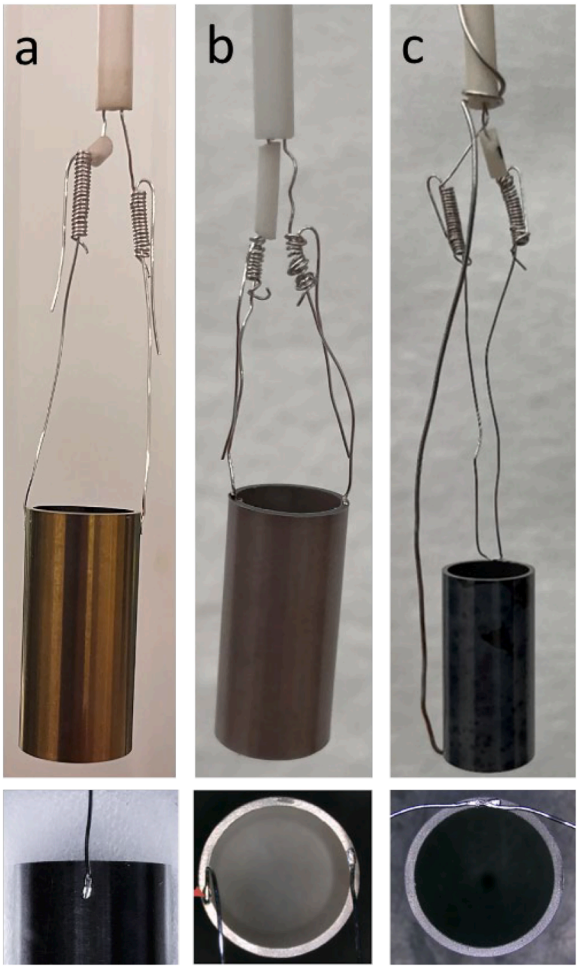

Fig. 2. a. Thermocouple welded on the lateral face (as received specimens). b and c. Thermocouple welded on the upper-end face (pre-oxidized specimens).

Table 3
Heating rates and temperature overshoots.

T (°C)	Heating rate for as-received cladding (°C/s)	Temperature overshoot (°C)	Heating rate with pre-ox tubes (°C/s)
900	15–16	No overshoot	14–16
1000	35–41	25–30	24–29
1100	59–60	60–85	38–41
1200	80–100	100–160	50

represents a significant enhancement of the TGA technique to better simulate LOCA oxidation conditions. This is particularly beneficial for pre-oxidized specimens because a slow, prolonged heating phase under argon gas flow, typically achievable on conventional TGA instruments, could lead to partial dissolution of the pre-oxidation layer. As a result, the obtained data would not be fully representative of LOCA scenarios with fast temperature rise.

With as-received tubes, a temperature overshoot was observed (see Fig. 3) as an effect of the massive exothermal energy release from the oxidation "shock" as the sample enters the furnace. At 1200 °C, this effect was quite pronounced, with an overshoot of up to 160 °C, but it lasted less than 20 s. No such overshoot was observed for pre-oxidized tubes.

2.4. Steam flow rate

Considering the test protocol used in the present study, where the experiment starts with the furnace open, a high Steam Flow Rate (FR) is required to prevent any air counterflow and undesired nitriding. Additionally, due to the high oxidation rate of zirconium-based cladding materials at high temperatures, fast renewal of the atmosphere around the sample surface is necessary, which also necessitates a high gas flow rate. Another prerequisite is easy access of the gas phase to the sample surface, including the inner surface. Under steam conditions, away from any breakaway influence, such as for short exposure times or above 1050 °C [14,29], the oxide scale formed remains dense, and hydrogen pick-up is not expected [34]. A high hydrogen content in the sample after oxidation would then indicate insufficient steam supply, as steam depletion and hydrogen enrichment of the atmosphere seen by the downflow part of the specimen surface would induce hydrogen incorporation there. This would affect oxidation kinetics because of slower oxidation of the parts of the surface experiencing oxygen starvation conditions. This effect is sometimes referred to as the "Hydrogen blanketing effect" [35]. Strong hydrogen pick-up was indeed reported after thermogravimetric oxidation tests by Steinbrück [28] as well as by Zino [29]. According to Steinbrück et al. [28], high hydrogen contents (up to 1500 wppm) were measured after the oxidation tests at 1100 °C (the highest temperature investigated in that work) for the four alloys studied (Zy-4, M5, E110, ZIRLO). The atmosphere was steam-rich (100 % steam), and the flow rate was rather high (5 g/h). However, difficult access of the steam to the inner surface of the tubes may be suspected due to the balance configuration (the specimens were not suspended but laid on a ceramic plate). In Zino's work [29], a SETARAM thermobalance was used, whose configuration was similar to the one used in the present study; however, the steam flow rates were very low (< 0.5 g/h). For the two alloys studied and for a relatively low temperature (1000 °C), hydrogen pick-up was reported (up to 1000 wppm) at the beginning of the steam exposure [36].

The effect of a low steam flow rate is illustrated in Fig. 4 for the M5 alloy at 1000 °C. TGA kinetic curves (i.e., derivative of the weight gain) from Zino [36], obtained for various flow rates in the range of 0.09 – 0.45 g/h, are compared to a test from the present study, obtained for a 58 g/h steam flow rate. A significantly higher oxidation rate peak is observed for the IRSN test, and later, from about 100–200 s, the rate becomes lower for the IRSN test. Plotting the rate as a function of the mass gain (or as a function of the scale thickness calculated from the mass gain assuming a fully dense oxide and considering that one-third of the oxygen mass is dissolved into the metallic substrate and doesn't contribute to the oxide growth [29]), the influence of the steam flow rate is even more visible. Above about 7 μm scale thickness, the oxidation rates measured by Zino are significantly higher than those determined from the present study, suggesting that hydrogen pick-up at the beginning of the tests may later affect the zirconia scale microstructure, resulting in a less passivating layer. One must also keep in mind that a low steam FR will favor non-homogeneous scale growth, which may complicate interpretation. A high steam FR is therefore preferable for unbiased kinetic measurements at high temperatures.

However, high FRs have been observed to have a negative impact on the temperature homogeneity inside the SETARAM thermobalance furnace. Additionally, at high steam flow rates, fluctuations of the TG signal were sometimes observed, likely due to condensation problems in the steam inlet pipe (see Fig. 5). A comparison at 1200 °C between tests performed at 100 g/h and 14.5 g/h steam flow rates (Fig. 5) shows a similar mass gain rate between the two tests. From the perspective of oxidation kinetics, a steam flow rate of 14.5 g/h is therefore deemed acceptable.

However, not only does the steam flow rate need to be considered, but also the potential for steam starvation may depend on many other parameters, such as the steam partial pressure, the specimen shape and size, the inner diameter of the furnace tube, etc. Additionally, any factor that may disrupt the gas flow around the specimen surface needs to be taken into account. A good parameter to check for potential steam starvation is the hydrogen pick-up. Therefore, the hydrogen content after high-temperature oxidation has been measured by hot extraction

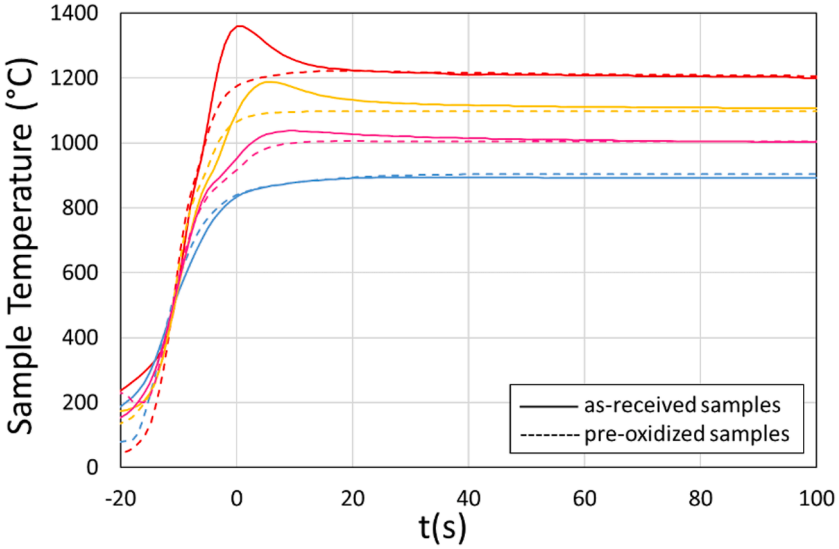

Fig. 3. Temperature profiles measured by the thermocouple welded on the sample.

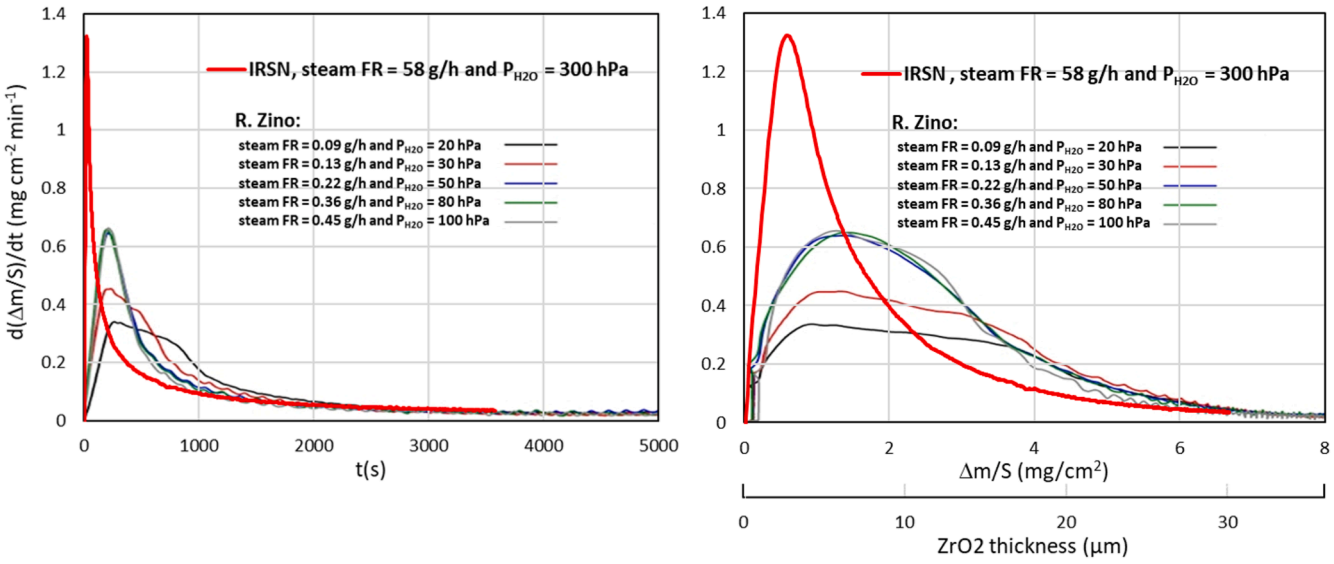

Fig. 4. Influence of the steam flow rate (FR) on mass gain rate. TGA oxidation tests at 1000 °C on as-received $M5_{Framatome}$. Mass gain rate plotted as a function of time (left) or as a function of mass gain and equivalent ZrO_2 thickness (right).

with a LECO instrument on selected Zy4 and M5 samples, corresponding to oxidation conditions for which hydrogen pick-up was not expected. The results are presented in Table 4. Most of the specimens have very low hydrogen content, confirming the absence of hydrogen pick-up during the high-temperature oxidation. Samples oxidized at 1200 °C with a steam flow rate of 14.5 g/h show a non-negligible amount of hydrogen incorporation. This indicates that this flow rate is insufficient to avoid steam starvation in the downstream part of the 20 mm long cladding tubes. However, the hydrogen contents remain moderate. More importantly, the consequence of the starvation on the oxidation kinetics appears to be negligible (see Fig. 5). Incidentally, these results show that for temperatures where breakaway oxidation may occur (900 and 1000 °C), none of the selected specimens have passed the breakaway transition, as their hydrogen content remains far below the 200 wtppm US-NRC breakaway criteria [34].

Finally, most of the tests in the present study were performed with a 14.5 g/h steam FR.

3. TGA résults

3.1. As received alloys

As-received Zircaloy-4 was investigated first to validate the experimental procedure. In Fig. 6, TGA data from the present work are compared to results obtained from interrupted tests (samples weighed before and after oxidation) conducted at Japan Atomic Energy Agency (JAEA) [9], KFKI Atomic Research Institute [37], Commissariat à l'Energie Atomique CEA [5,38], and at IRSN [7,39], all performed with low-tin Zircaloy-4 material. Interrupted tests from IRSN were associated with post-test hydrogen content measurements to ensure that they were not biased by steam starvation and are considered as a reference for this comparison. A generally good agreement between TGA tests and interrupted tests is observed. It is worth noticing the very good reproducibility of the TGA tests (5 tests performed at 1000 °C and 3 tests at 1200 °C) while significantly higher scattering is observed for interrupted tests. Fig. 6 also depicts the predictions, for temperatures of 1000, 1100, and 1200 °C, made with the Cathcart-Pawel correlation, derived from tests

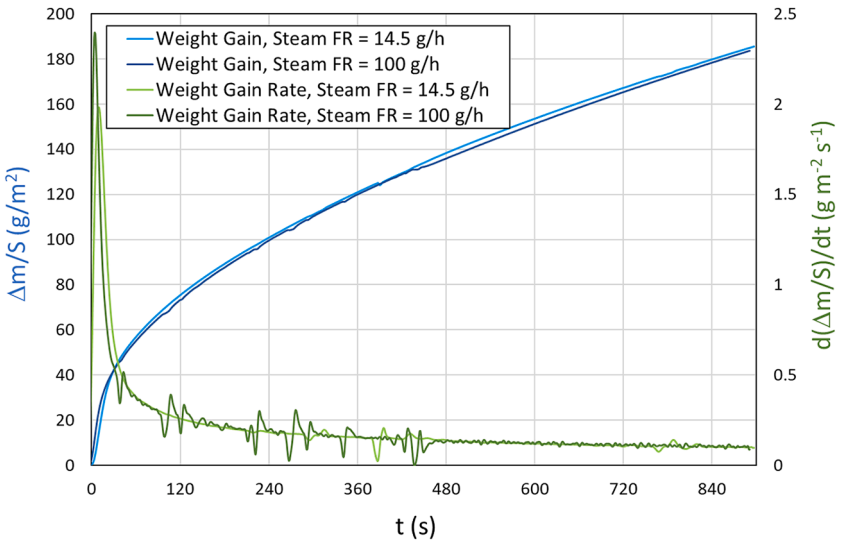

Fig. 5. TGA tests on as-received M5 at 1200 °C for two different steam FR.

Table 4
Hydrogen content after HT oxidation.

Alloy	Oxidation temperature (°C)	Steam flow rate (g/h)	Duration (min)	H content (wtppm)
Zy4	900	14.5	60	16 ± 5
	1000	14.5	60	36.5 ± 10
	1000	14.5	60	24.5 ± 7
	1100	14.5	30	17 ± 5
	1200	**14.5**	**15**	**184.5** ± 25
	1200	**14.5**	**15**	**101**± 15
M5	900	58	30	4.5 ± 3
	1000	58	60	8.5 ± 3
	1000	58	60	5 ± 4
	1100	58	30	14 ± 5
	1100	14.5	30	15.5 ± 5
	1200	100	15	11.5 ± 4
	1200	**14.5**	**15**	**128.5** ± 40

using high-tin Zircaloy-4 [40]. The predictions tend to overestimate the TGA data and appear to be an upper bound of the interrupted tests.

The present TGA results on Zy4 were compared to TGA data from the Karlsruhe Institute of Technology (KIT) [28] and from Korea Atomic Energy Research Institute (KAERI) [25] (Fig. 7). For clarity, only one test from the present study is plotted at each temperature. It's worth noting that the KIT TGA curves have been corrected before plotting: in Fig. 2 of Ref. [28], a steep increase at $t = 0$ when steam is injected into the thermobalance can be systematically observed on all weight gain curves at 900 °C, 1000 °C, 1100 °C, and 1200 °C. This effect is believed to be due to a hydrodynamic effect when steam is injected into the thermobalance furnace and has been subtracted from the published original curves. Except at 900 °C, rather significant discrepancies are observed between the three studies. As discussed in the "Steam Flow Rate" section, steam starvation likely occurred during the KIT tests, which may have impacted the oxidation kinetics. Furthermore, the experimental procedures also differ significantly between the three laboratories. Finally, Zy4 batches can differ in composition and surface finish, which may also contribute to the observed variations.

The same type of comparative analysis has been conducted with as-received M5. In Fig. 8, TGA curves from the present study are compared

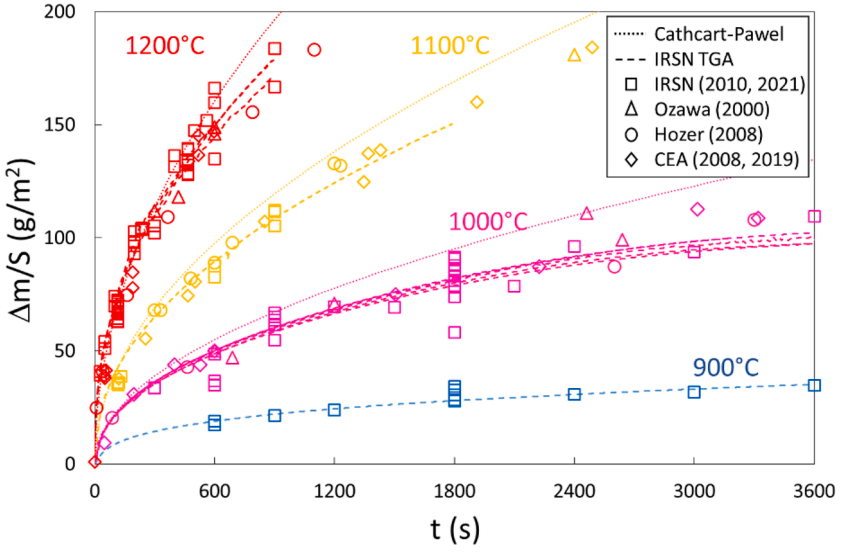

Fig. 6. Results on as-received Zy-4. TGA data compared to interrupted test results from JAEA [9], KFKI [37], CEA [5,38] and IRSN [7,39].

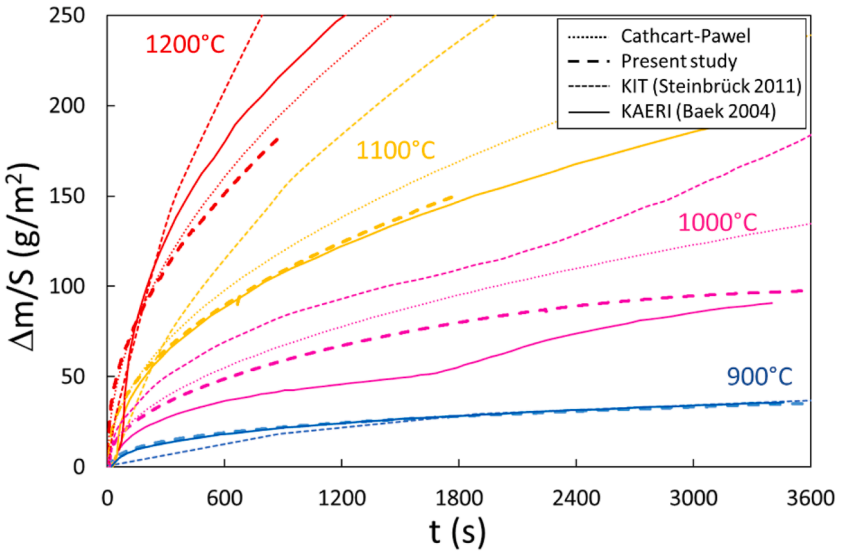

Fig. 7. TGA results on as-received Zy-4. Data from the present study compared to data from KIT [28] and from KAERI [25].

to results of interrupted tests obtained at CEA [5], JAEA [41], and IRSN, as well as with TGA data from KIT [28]. Similar to Zy4, KIT TGA curves have been corrected before plotting. Once again, the IRSN TGA measurements demonstrate good reproducibility (two tests are plotted at 1000 °C, 1100 °C, and 1200 °C), and a notable agreement with data points from interrupted tests is observed. The differences between KIT and IRSN TGA curves are less pronounced compared to Zy4 but still noticeable, likely attributable to differences in test protocols and steam flow rates.

For the present study, high-temperature oxidation of as-received Optimized ZIRLO was investigated in greater detail compared to Zy4 and M5, primarily due to the limited availability of data in the open literature for this alloy. Specifically, longer tests were conducted, and additional temperatures were explored around 1000 °C, where breakaway oxidation typically occurs. TGA curves obtained with Optimized ZIRLO specimens are illustrated in Fig. 9. Once again, the data exhibit good reproducibility, with tests repeated at 950 °C, 975 °C, 1000 °C, 1050 °C, and 1100 °C. Over the duration investigated, breakaway transitions were observed at 975 °C, 1000 °C, 1025 °C, and 1050 °C. Breakaway times were determined from the minima of the time derivative of the weight gain curves, providing unambiguous and accurate values. The results are depicted in Fig. 10. It is noteworthy that at 975 °C and 1000 °C the breakaway time remained consistent for the two tests conducted. These findings are consistent with data found in the open literature for ZIRLO, confirming that the minimum breakaway time typically occurs around 1000 °C, as also commonly observed for Zy4. Due to the much earlier breakaway observed at 1000 °C and 1025 °C compared to 1050 °C, the mass gain curves at 1000 °C and 1025 °C surpass the curve at 1050 °C for longer durations.

TGA weight gain curves obtained with as-received specimens are compared for the three alloys in Fig. 11, for times < 3600 s. At 1100 °C and 1200 °C, all the curves merge, indicating no difference in oxidation kinetics between the alloys. However, at 1000 °C, the weight gains vary significantly among the alloys, following the order: Zy4 > OZ > M5. In this study, due to the earlier breakaway for Optimized ZIRLO (2000s) compared to Zy4 (3800 s), the weight gain for OZ surpasses that of Zy4 for exposure times > 4500 s. This behavior has also been observed by Steinbrück et al. with ZIRLO [28]. However, it's important not to generalize this observation because the breakaway time for a given alloy may depend on various parameters such as batch composition, surface

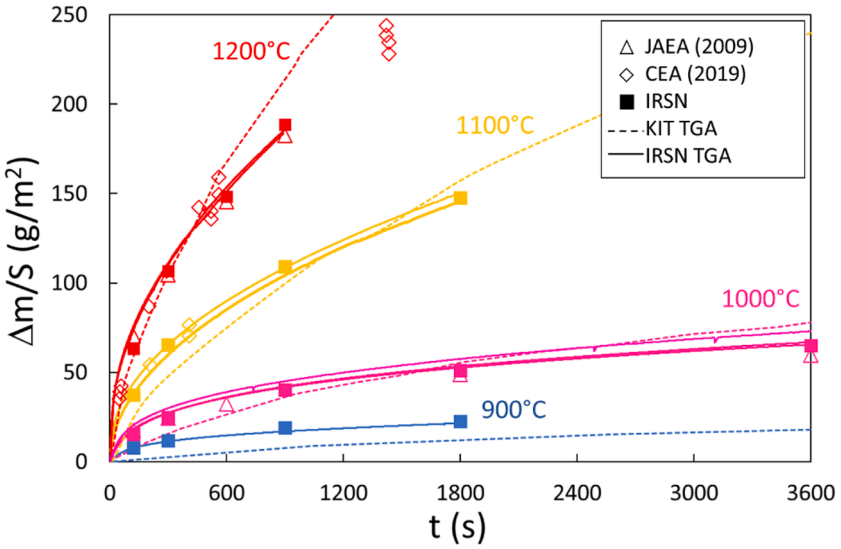

Fig. 8. Results on as-received M5. TGA data compared to interrupted data points from CEA [5] and JAEA [41], and to TGA data from KIT [28].

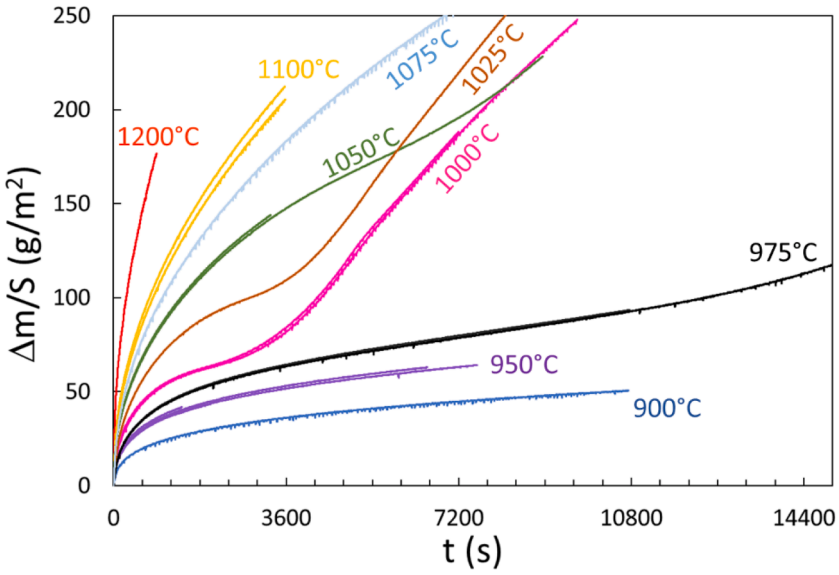

Fig. 9. Weight gain curves obtained with as-received Optimized ZIRLO specimens.

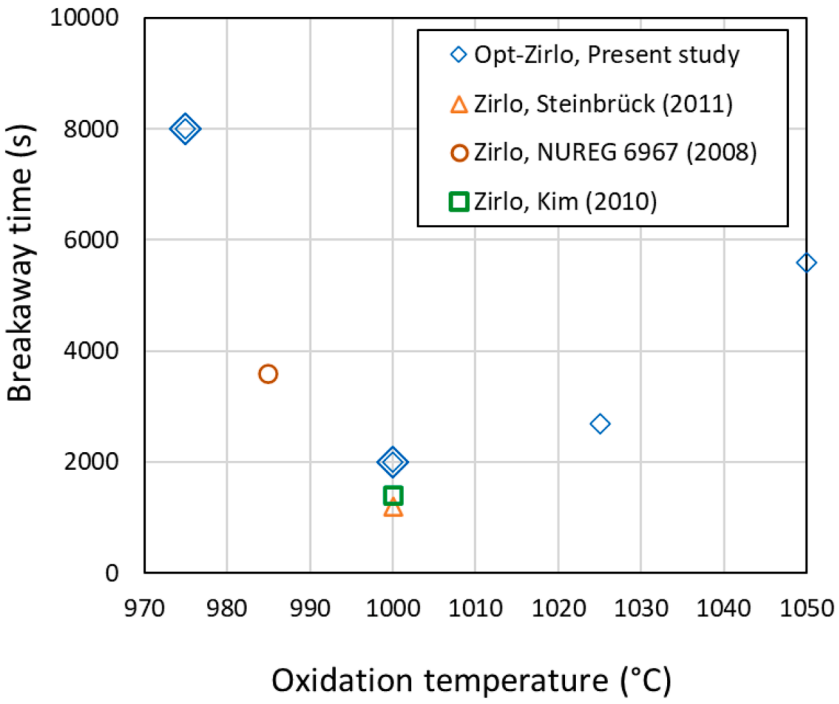

Fig. 10. Breakaway time for Optimized ZIRLO (present study) and for ZIRLO (NUREG 6967 (2008) [42], Kim (2010) [31], Steinbrück (2011) [28]).

state, steam flow rate, etc. Breakaway times at 1000 °C ranging from 1500 to 5700 s have been reported for Zy4 [36]. For M5, no breakaway transition has been reported with recent batches, even after very long exposures (10,000 s [5] or even 16,000 s [36]). In this study, no breakaway transition for M5 was observed at 1000 °C up to a test duration of 10,000 s. At 900 °C, TGA curves merge for Zy4 and Optimized ZIRLO, while the kinetics are slightly slower for M5. This confirms the earlier observation by Mardon and Dunn [33] regarding the better behavior of M5 compared to Zy4 at intermediate temperatures.

For all temperatures investigated and for the three alloys, experimentally measured mass gains are consistently lower than mass gains calculated from the Cathcart-Pawel correlation [43]. In other words, the Cathcart-Pawel correlation is deemed to be a conservative approach for calculating zirconium alloy oxidation kinetics in steam at high temperatures.

3.2. *Pre-oxidized specimens*

In the case of pre-oxidized specimens, solely the lateral inner and outer surfaces are covered by an oxide layer. The end surfaces remain uncovered, either due to the 20 mm samples being cut from longer pre-oxidized tubes or, in instances where samples were cut to 20 mm prior to pre-oxidation, because the end faces were polished subsequent to pre-oxidation for thermocouple welding purposes. To ensure that the mass measurements accurately reflected the pre-oxidized surfaces, a correction was systematically applied to subtract the contribution of the end

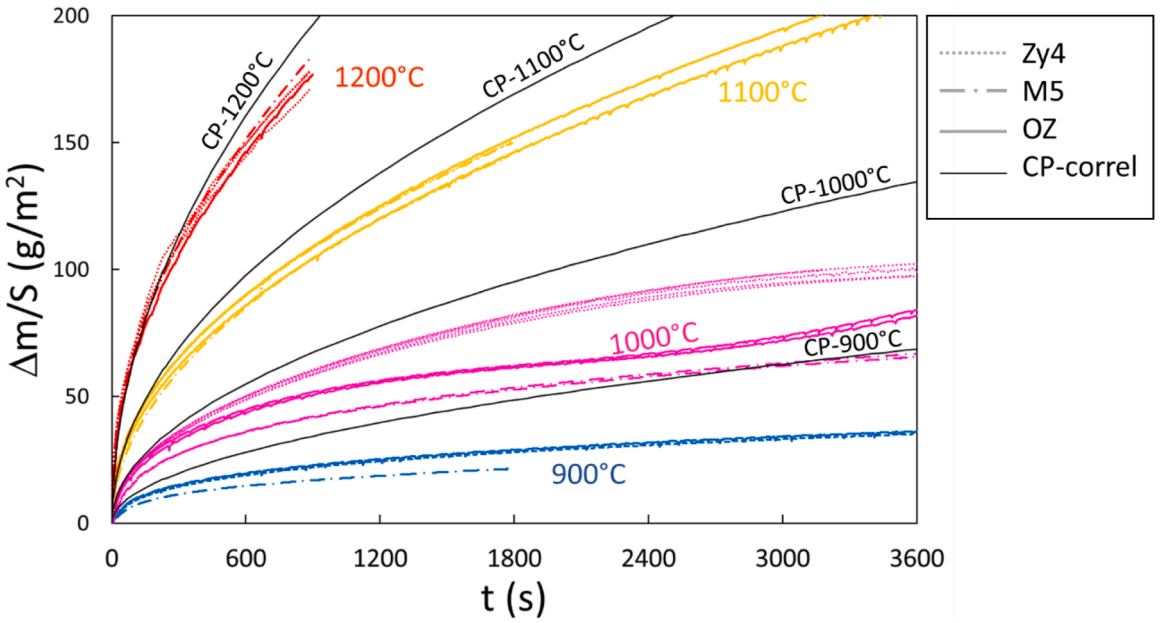

Fig. 11. Comparison of Weight gain curves obtained with as-received Zircaloy-4, M5 and Optimized ZIRLO at 1200, 1100, 1000 and 900 °C. At each temperature, the Cathcart-Pawel (CP) correlation [43] is also plotted (black lines).

faces. This correction was based on the mass gain results obtained from the as-received samples:

$$(\Delta m/S)_{corr} = \left[\Delta m_{\exp} - (\Delta m/S)_{as-received} * S_{ends}\right]/S_{lat} \quad (1)$$

where Δm_{exp} is the experimentally measured weight gain, $(\Delta m/S)_{as\text{-}received}$ is the weight gain per area unit for as-received samples, calculated from $(Kt)^{1/n}$ fits (see the discussion section)

S_{ends} is the area of both end faces

S_{lat} is the area of lateral inner and outer surfaces

Additionally, during tests conducted at temperatures of 1000 and 1100 °C on pre-oxidized Zy4, featuring a 30 μm thick pre-oxidation scale, a pronounced edge effect was observed (refer to (Fig. 12). This effect denotes the onset of high-temperature oxidation at the tube edges, succeeded by axial propagation of oxidation beneath the pre-oxide layer [32]. This phenomenon is clearly discernible in the metallography. To account for this effect in mass measurements, corrections were made,

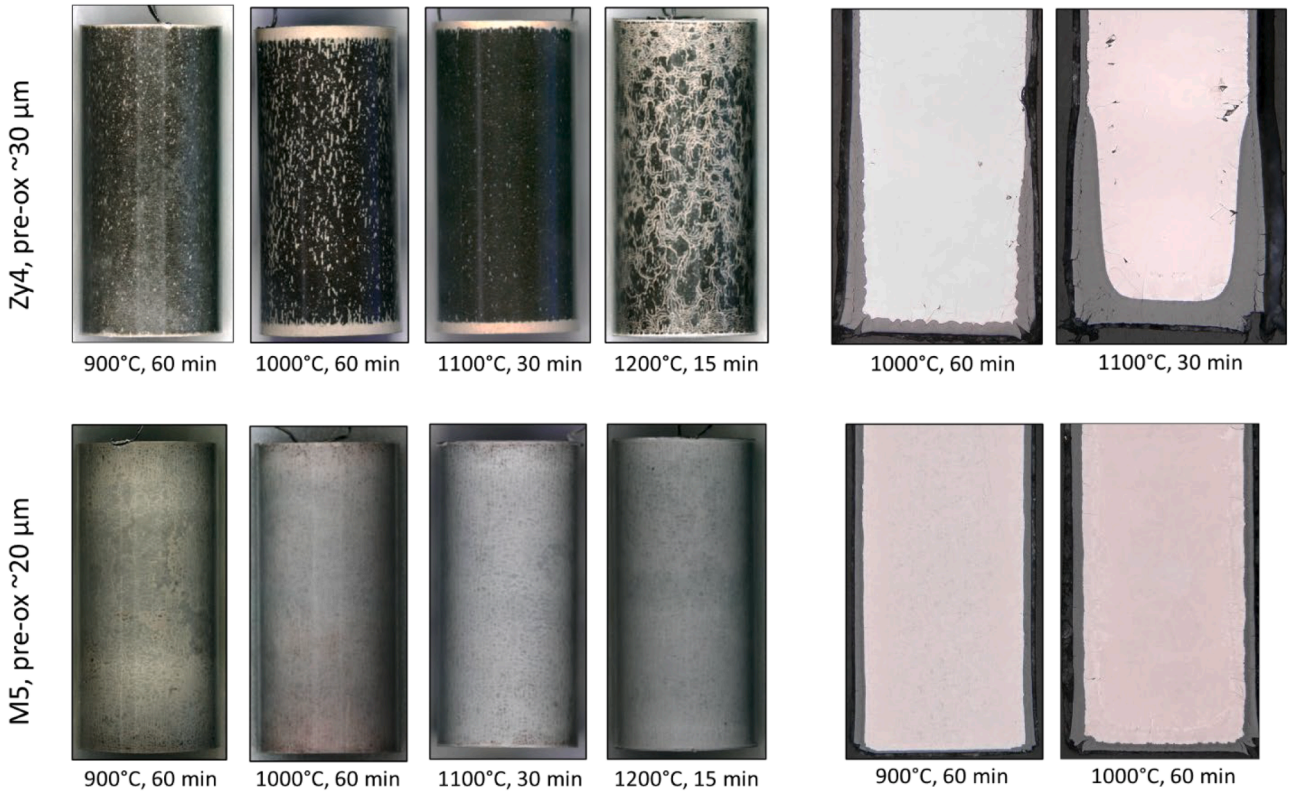

Fig. 12. Pre-oxidized specimens after high temperature oxidation and axial metallographic cross sections of the end of selected specimens.

considering the following factors: i) axial propagation from the edges occurring at a constant speed, V. By evaluating the axial extension of the affected zone at the test's conclusion (Fig. 13b), V was estimated to be 0.22 μm/s at 1000 °C and 0.35 μm/s at 1100 °C; ii) within the region affected by this propagation, oxidation kinetics align with those of the as-received samples, determined from $(Kt)^{1/n}$ fits (refer to the discussion section). Hence, the contribution of the edge effect to the measured mass gain, which necessitates subtraction, can be expressed as:

$$\Delta m_{edge\ \ effect} = 2 * V * \pi(D_{in} + D_{out}) \int_0^t kt^{1/n} dt \quad (2)$$

where D_{in} and D_{out} are the inner and outer diameters of the cladding tubes, respectively.

Finally, for the tests conducted at 1000 and 1100 °C with pre-oxidized Zy4, the measurements require double correction—once for the contribution of the end surfaces and once for the edge effect:

$$(\Delta m/S)_{corr} = \left[\Delta m_{\exp} - (\Delta m/S)_{as-received} * S_{ends} - \Delta m_{edge\ \ effect}\right]/S_{lat} \quad (3)$$

These corrections, addressing both the contributions from end faces and edge effects, yield notable changes in the raw measurements, as depicted in Fig. 13. Particularly, the correction for the edge effect becomes significant for prolonged oxidation durations. To validate the correction derived from Eq. (2), the volume of oxide formed at high temperature beneath the pre-oxide layer at the ends was evaluated through metallography conducted on an axial section of a specific specimen. The volume of the high-temperature oxide was estimated from the area of the triangles outlined in red in Fig. 13b, and subsequently, the mass of this high-temperature oxide was deducted from the final mass, resulting in the point depicted in green in Fig. 13a. This outcome serves to confirm the validity of the correction proposed by Eq. (2). In the case of M5 specimens, despite a minor color alteration at the ends of the samples, metallographic analyses reveal that the edge effect was minimal and thus does not necessitate correction.

TGA results obtained with pre-oxidized specimens are depicted as dotted lines in Fig. 14 and Fig. 15 for Zy4 and M5, respectively. These results are compared with TGA curves obtained from as-received specimens (displayed as full lines) as well as with data points acquired from interrupted tests on the OHTAVA furnace using pre-oxidized specimens, as reported in [7] for Zy4, and not previously published for M5. In the case of Zy4, TGA tests were conducted with 30 μm thick pre-oxide layers, confirming the strong protective influence observed throughout the interrupted tests. At 1200 °C, this protective effect is less effective. A good agreement between TGA and interrupted tests results is observed. For M5, the scenario is more intricate due to the variation in pre-oxide thicknesses and pre-oxidation conditions tested. Nonetheless, there is still an evident protective influence of the pre-oxidation layer, which amplifies with increasing pre-oxide thickness but also varies based on the pre-oxidation conditions. Particularly, under pre-oxidation conditions with higher steam partial pressure, resulting in the incorporation of elevated hydrogen amounts during pre-oxidation, the protective influence of the pre-oxide scale is weakened. Despite no clear explanation for this effect due to the absence of discernible differences in the microstructures of the pre-oxidation scales observed in SEM images, specimens with lower hydrogen incorporation levels are presumed to be more indicative of in-reactor corrosion. Interrupted tests were conducted with specimens pre-oxidized under lower steam partial pressure conditions, resulting in lower hydrogen incorporation levels (30, 45, and 60 wtppm for pre-oxide scale thicknesses of 5, 10, and 20 μm, respectively), and should thus be compared to TGA tests performed with the same type of specimens. Overall, the agreement between the two sets of tests appears satisfactory.

4. Discussion

4.1. Kinetic analysis of the pre-breakaway regime for as-received claddings

It is widely recognized that the oxidation of Zr alloys follows an internal oxidation process, wherein the new oxide forms at the metal/oxide interface and is predominantly governed by oxygen diffusion through the evolving zirconia scale, as far as the scale remains dense, meaning away from breakaway oxidation. Traditionally, the oxidation kinetics of Zr alloys at high temperatures are assumed to be parabolic [40]. However, previous studies have documented notable deviations from this parabolic regime [25,36,44], suggesting that the kinetic regime can be more accurately described by employing a variable *n* exponent, rather than adhering to a fixed value of 2 in the following equation:

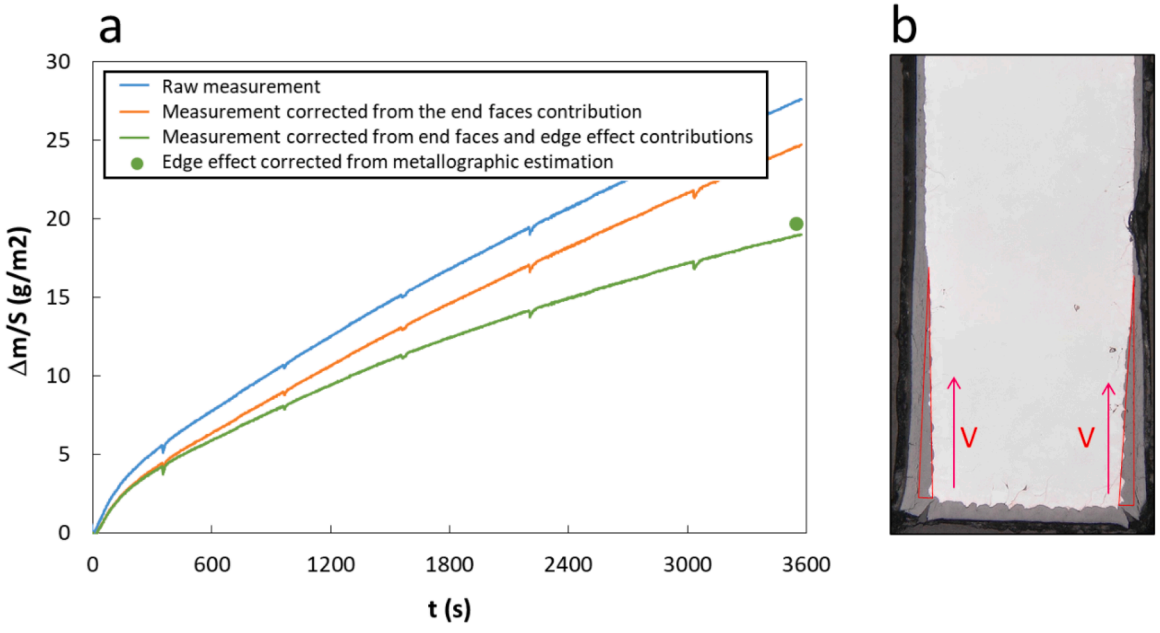

Fig. 13. a- TGA mass gain curves for a Zy-4 pre-oxidized specimen oxidized at 1000 °C, showing the end faces and edge effect corrections. b- Axial metallographic cross section of the specimen's end from which the mass of high temperature oxide formed by edge effect was estimated.

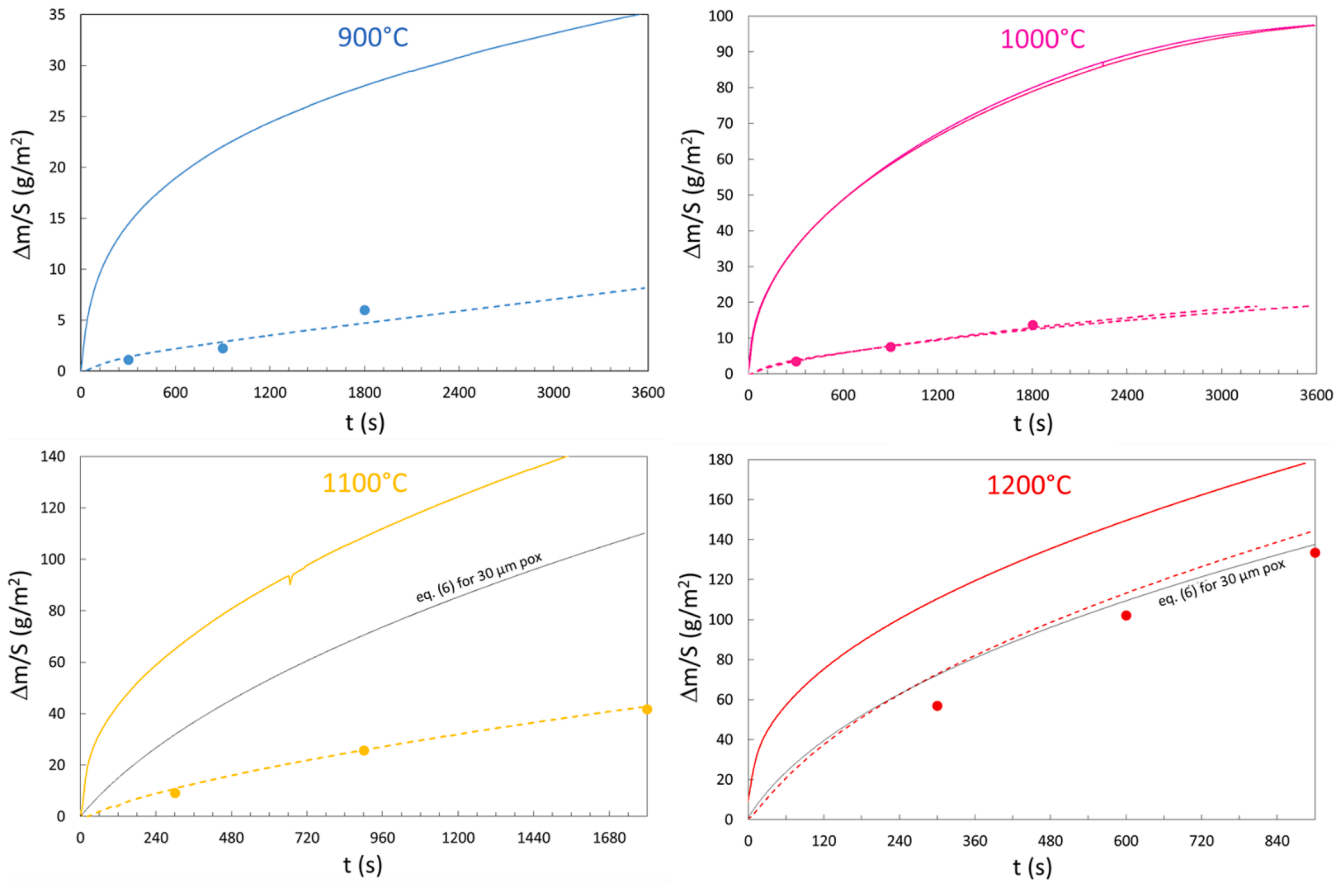

Fig. 14. TGA weight gain curves for 30 µm pre-oxidized Zy4 specimens (dotted lines) compared to the curves for as-received Zy4 (full lines). Data points obtained from interrupted tests with 30 µm pre-oxidized Zy4. Black lines calculated from Eq. (6), see the discussion section.

$$\Delta m / S = (Kt)^{1/n} \tag{4}$$

where K is a constant depending on the temperature.

Weight gain curves from the current study were fitted to Eq. (4) utilizing the Excel solver. Data points for the initial 100 s were excluded from the fit due to the incomplete stabilization of temperature at the onset of the tests. Given that the shortest breakaway time observed was 2000s (at 1000 °C for OZ), the fits were initially constrained to a maximum time of 1800s for consistency across all three alloys. However, it was noted that the results for OZ at 1000 °C exhibited significant variation when the maximum time considered was reduced to 1200s. Consequently, to eliminate any potential influence of the breakaway transition on the 'n' and 'K' parameters, a time range of 100–1200s was selected for the fits. For tests conducted at 1200 °C, the time range was 100–900 s.

Examples of fits at 1000 °C are illustrated in Fig. 16 for the three alloys. For Zy4 and OZ, as the breakaway transition approaches—at 2000s for OZ and 3800 s for Zy4—a pronounced deviation from the fit extrapolation is noticeable, indicating a significant deceleration of the mass gain rate prior to the occurrence of the breakaway transition. This deceleration phenomenon has previously been documented for ZIRLO by Lee and colleagues, who proposed that the formation of porosities at the metal/oxide interface contributes to the slowdown [45]. Indeed, voids are observed at the M/O interface following 3600 s of oxidation at 1000 °C for Zy4 (refer to Fig. 17a). The distribution of voids appears to correlate with the undulation of the M/O interface: voids are predominantly present where the oxide scale is thinner, implying that they impede the inward progression of the oxide and may be accountable for the deceleration in weight gain. Conversely, such voids are not observed for M5 after 3600 s at 1000 °C (refer to Fig. 17b); no breakaway transition was noted within the extended test duration (10000s), and the experimental mass gain curve exhibits only a slight deviation from the $(K\,t)^{1/n}$ fit. Unfortunately, no metallographic image is available for OZ as no test at 1000 °C was interrupted prior to the breakaway transition.

The values of the parameters n and K derived from the fits are presented in Table 5. The values of n are depicted in Fig. 19 and compared with literature values obtained from TGA experiments [25,31,36], as well as values from interrupted tests conducted on Zy4 at JAEA [44] and on M5 at IRSN (not yet published). While acknowledging potential variations in experimental conditions across studies, particularly in steam flow rate, and recognizing that the fit output depends on the time range considered, the agreement between literature data and values from the current study is deemed satisfactory. Generally, it is observed that n values are approximately close to 2 at high temperatures, whereas at lower temperatures, the n exponent tends to increase, reaching values in the 2.5 - 3 range. This trend aligns with observations from previous studies [25,31,36]. The transition from a sub-parabolic ($n > 2$) to a near-parabolic ($n \approx 2$) regime with increasing temperature appears to occur rather abruptly. Hence, our data were fitted using an arctangent-type function (refer to Fig. 18):

$$n = n_{min} + \left(\frac{n_{max} - n_{min}}{2}\right)\left(1 - 2\pi\ arctangent\left(\frac{T - T_0}{\beta}\right)\right) \tag{5}$$

Where n_{max} and n_{min} are the max and min n values
T the temperature
T_0 the temperature at which the transition occurs
2β (in K) is the width to go from 25 to 75 % of the $n_{min} - n_{max}$ interval.
n_{min}, n_{max}, T_o and β values derived from the fits are given in Table 6.

The fits, depicted as dotted lines in Fig. 19, suggest that the transition from a sub-parabolic ($n > 2$) to a nearly parabolic ($n \approx 2$) regime occurs

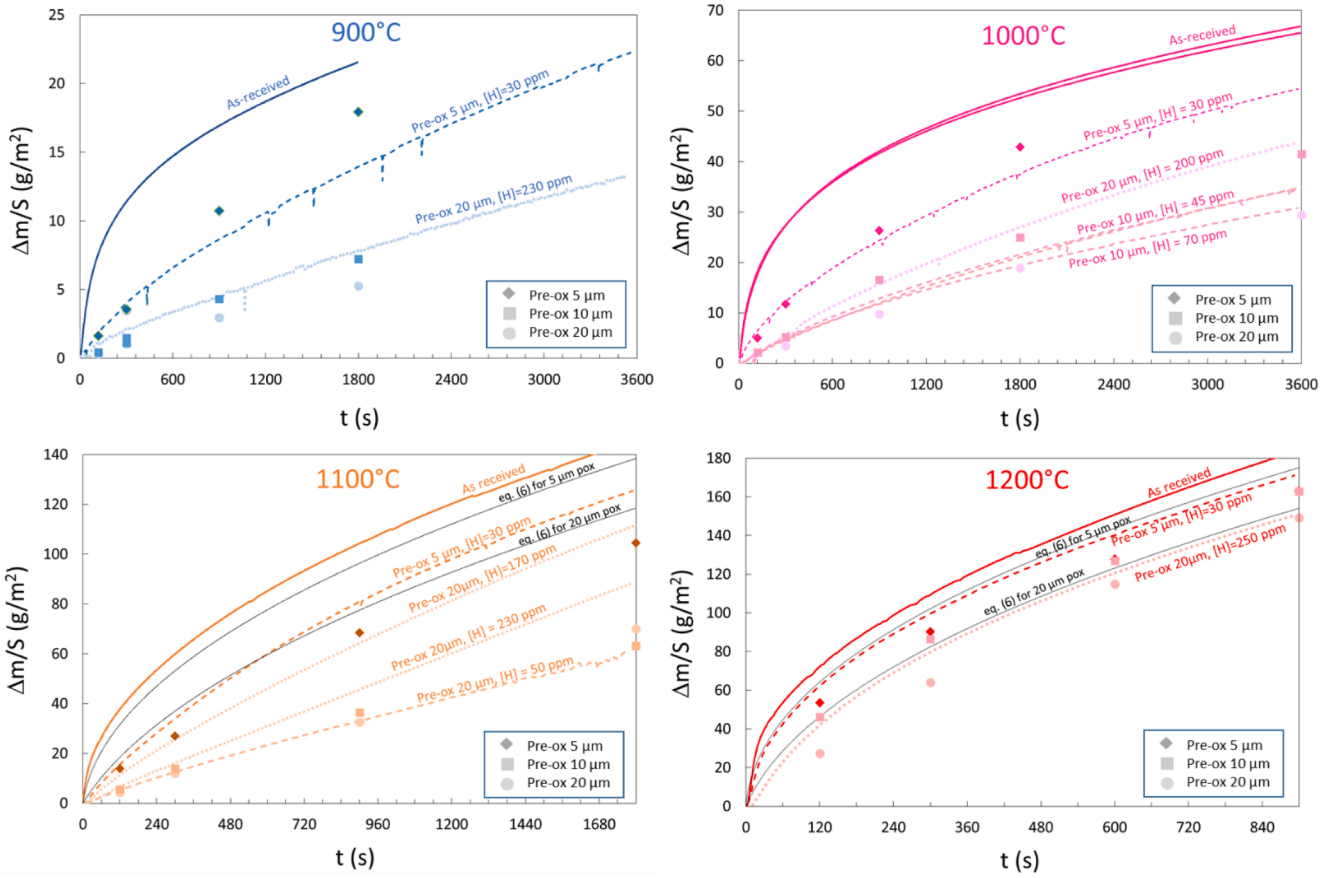

Fig. 15. TGA weight gain curves for pre-oxidized M5 specimens (dotted lines) compared to the curves for as-received M5 (full lines). Data points obtained from interrupted tests with pre-oxidized M5. Black lines calculated from Eq. (6), see the discussion section.

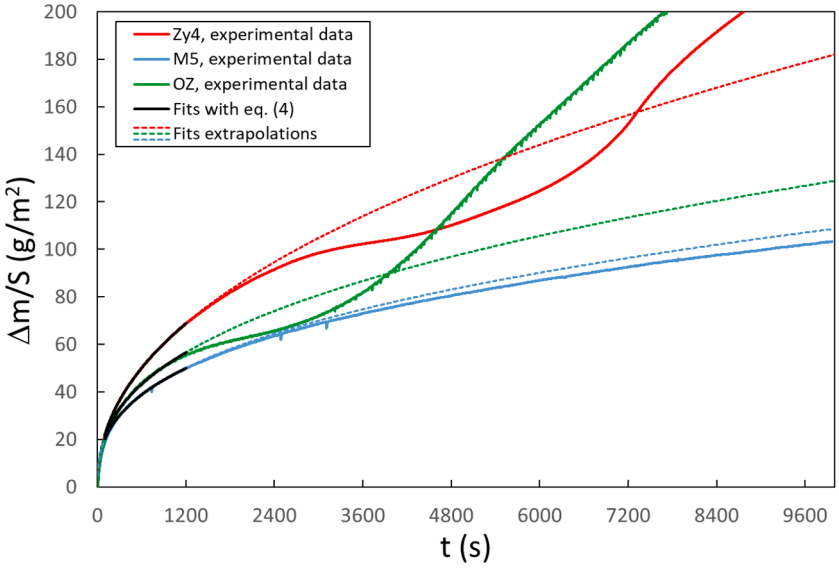

Fig. 16. TGA weight gain curves and fits with Eq. (4) for tests at 1000 °C.

at higher temperatures (above 1000 °C) for the Nb-bearing alloys compared to Zircaloy-4.

Theoretically, the so-called parabolic kinetic regime ($n = 2$) implies that the oxygen diffusivity in zirconia remains constant over time [46]. Deviations from the parabolic regime below 1000 °C were initially observed for Zy4 by Suzuki and co-workers [24] and subsequently confirmed by numerous authors [25,44,47]. An exponent n greater than 2 likely indicates a decrease in oxygen diffusivity over time during scale growth, although there is no consensus on the underlying causes of this decrease. Compressive stresses and the tetragonal to monoclinic phase transformation of zirconia are frequently cited as potential factors contributing to the deviation from the parabolic regime, and these effects may be coupled. Several studies have demonstrated that compressive stresses develop in thermally grown zirconia scales due to

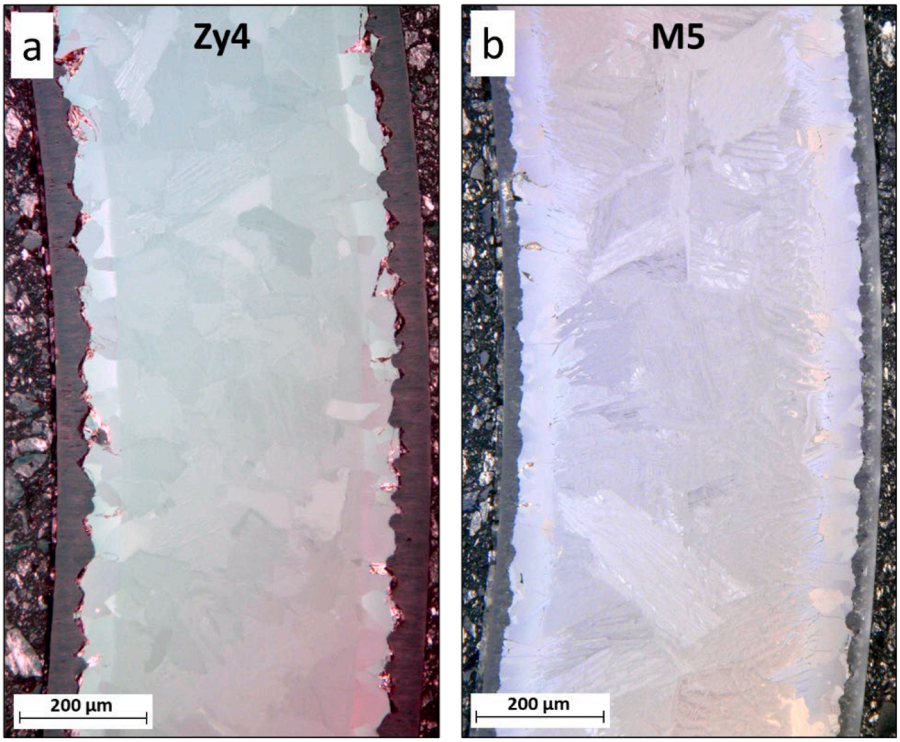

Fig. 17. Radial cross sections of Zy4 and M5 specimens after 3600 s oxidation at 1000 °C. Inner and outer sides of the tubes are to the left and to the right respectively.

Table 5
K and n values inferred from fitting experimental weight gain data to Eq. (4) in the 100–1200s time range.

Alloy	T (°C)	K ($g^n\ m^{-2n}\ s^{-1}$)	n
Zy4	900	3.64	2.61
	1000	8.03	2.18
	1000	8.46	2.20
	1000	8.96	2.20
	1000	7.88	2.16
	1000	8.44	2.18
	1100	24.04	2.13
	1200	426.4	2.50
	1200	330.4	2.43
	1200	145.9	2.27
M5	900	3.26	2.82
	1000	20.85	2.64
	1000	17.02	2.58
	1100	8.88	1.93
	1100	29.00	2.17
	1200	78.68	2.14
	1200	84.86	2.15
OZ	900	4.93	2.69
	950	17.29	2.74
	950	21.67	2.80
	950	15.50	2.69
	950	25.52	2.80
	975	11.53	2.49
	975	11.11	2.49
	1000	33.25	2.63
	1000	27.44	2.58
	1025	12.10	2.21
	1050	18.10	2.20
	1050	17.57	2.20
	1075	15.05	2.09
	1100	19.66	2.10
	1100	24.16	2.13
	1200	74.58	2.15

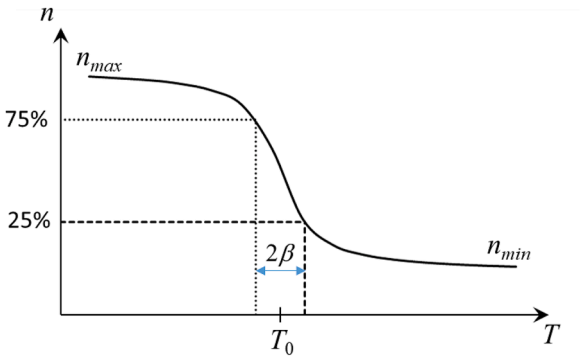

Fig. 18. Arctangent function used to fit $n = f(T)$ data.

Table 6
n_{min}, n_{max}, T_0 and β parameters derived from fits of n values with eq. (5).

Alloy	n_{min}	n_{max}	T_0 (K)	β (K)
Zy4	2.13	2.65	1250	10
M5	2.12	2.86	1287	10
OZ	2.15	2.74	1281	5.7

the relatively high Pilling-Bedworth ratio of the Zr/ZrO_2 system (readers could refer to the review paper [48]). Although most of these studies pertain to normal operating temperatures, a few studies conducted under higher temperature conditions [49,50] confirm the existence of compressive stresses in the zirconia scales. Spatially resolved measurement techniques often indicate the presence of a stress gradient across the scale, with maximum compressive stresses occurring near the metal/oxide interface [50-53]. Compressive stresses are known to stabilize the tetragonal phase of zirconia (t-ZrO_2) [51,54] below its stability temperature range (~1205–2377 °C for stoichiometric zirconia [55]). Hypostoichiometry (i.e., oxygen vacancies in the anion sublattice) also

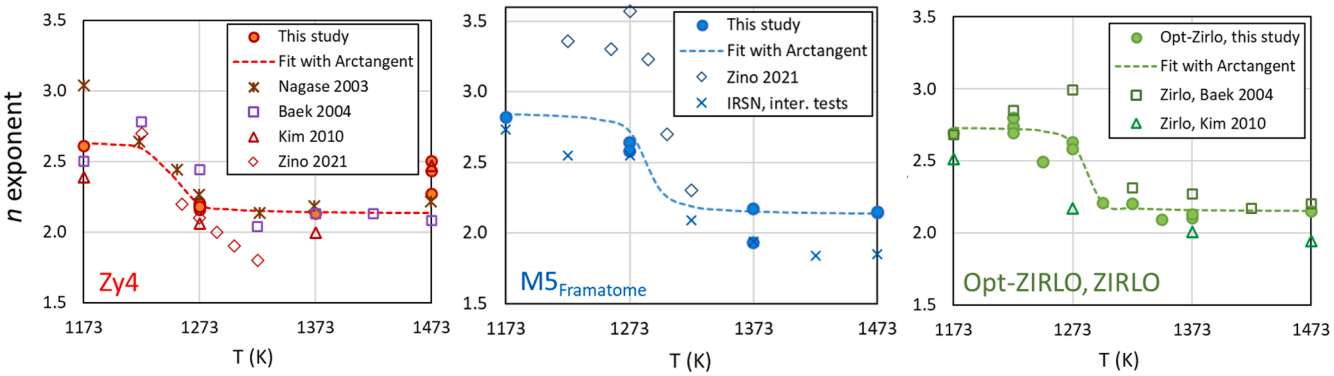

Fig. 19. Exponent n inferred from Eq. (4). Comparison with TGA data from, Baek et al. [25], Kim et al. [31] and Zino [36], and with interrupted tests data from Nagase et al. [44] and interrupted test data from IRSN. Dotted lines are fits of our data points with eq. (5).

contributes to the stabilization of t-ZrO2 at low temperatures [56]. Consequently, as evidenced by Raman investigations [50,51], t-ZrO_2 is likely to form near the M/O interface below 1200 °C, where both the level of compressive stress and the deviation from stoichiometry are high. As the oxide scale grows, t-ZrO_2 grains formed at the interface move away from the interface and tend to convert into monoclinic zirconia (m-ZrO_2). Therefore, it is understood that the proportion of t-ZrO_2 in a scale decreases relative to m-ZrO2 as the scale grows, a phenomenon well established by in-situ XRD studies [57-59]. Since the oxygen diffusivity is several orders of magnitude lower for m-ZrO_2 [60,61] than for t-ZrO_2 [62,63], this would result in a decrease in the apparent mean oxygen diffusivity of the scale over time and consequently an exponent *n* greater than 2. Zino and colleagues [59], utilizing Zircaloy-4 substrate, have reported that above 1000 °C, the fraction of t-ZrO_2 remains constant over time, consistent with an exponent *n* approximately equal to 2.

4.2. *Effect of pre-oxidation*

All TGA curves obtained with pre-oxidized specimens show mass gain as soon as the sample is heated, with the mass gain rate continuously decreasing over time, for all temperatures investigated and for both Zy4 and M5. While this behavior aligns with the formation of a protective layer on bare alloys, it is unexpected for pre-oxidized cladding specimens. Specifically, given the pre-oxidation conditions examined in this study, the pre-oxidized scales formed have been predominantly observed to be stoichiometric [7]. Consequently, one would anticipate an initial phase with minimal or negligible mass gain rate at the onset of the high-temperature stage, corresponding to the time needed to establish a gradient of oxygen vacancies across the pre-oxide layer. Such a gradient is necessary to allow new oxygen incorporation and subsequent diffusion towards the metal/oxide interface. However, the TGA data demonstrate that oxygen is indeed incorporated from the outset of the high-temperature plateau.

At first glance, one might suggest a rapid oxygen gas phase transport process through open porosities within the pre-oxidized layer. However, this contradicts the markedly lower mass gain rate observed for pre-oxidized specimens compared to bare ones. Moreover, this explanation is inconsistent with data previously obtained at 850 °C using ^{18}O as a diffusion tracer, which indicated a limited contribution from the porosity network in the pre-oxidized layer to oxygen transport [64]. Instead, it should be considered that oxygen diffusion from the pre-oxidized layer to the underlying metal, along with the concurrent growth of a thick α-Zr(O) layer, occurs as the temperature increases. Oxygen vacancies are subsequently generated in the oxide layer close to the metal, ultimately leading to oxide-to-metal conversion [7,32]. Therefore, rapid diffusion of vacancies and the establishment of an oxygen vacancy gradient across the pre-oxidized scale could elucidate the incorporation of new oxygen from the gas phase right from the initiation of the high-temperature stage.

When discussing the role of a pre-oxidized layer in high-temperature oxidation, it's also essential to consider the influence of crystallographic phases of zirconia. Zirconia layers grown at 425 °C have been predominantly observed to consist of the monoclinic phase, at least after cooling to room temperature, as evidenced by Raman mapping [7,64]. Conversely, the tetragonal phase predominates at high temperatures, with only tetragonal zirconia (t-ZrO_2) grains forming above 1100 °C [57,58]. Since the oxygen diffusivity is significantly lower for monoclinic zirconia (m-ZrO_2) compared to tetragonal zirconia (t-ZrO_2), the crystallographic composition (at high temperatures) of both the pre-existing low-temperature zirconia layer and the growing high-temperature scale could impact the kinetics of high-temperature oxidation. To shed light on this aspect, a theoretical mass gain was calculated under the assumption that the pre-oxidized layer offers the same passivation effect as a high-temperature oxide scale with an equivalent d thickness. Utilizing the $kt^{1/n}$ adjustments derived from the TGA curves obtained on as-received samples, the mass gain can be expressed as follows:

$$(\Delta m/S)(t) = [K(t+t_1)]^{1/n} - [Kt_1]^{1/n} \quad (6)$$

where t_1 represents the time required to form a scale of thickness δ at high temperature.

This calculation holds physical significance only if the oxygen diffusion coefficient remains constant as the oxide thickness increases, implying parabolic kinetics. As such, it was conducted at 1100 °C and 1200 °C only, where the *n* coefficient was close to 2. The curves calculated by Eq. (6) have been plotted as black lines in Fig. 14 and Fig. 15. At 1200 °C, these calculated curves appear to correspond quite well with experimental data obtained from pre-oxidized specimens, indicating that the pre-oxidized layer provides the same protective effect as a scale of equivalent thickness formed at 1200 °C. In other words, oxygen diffusion through both the low-temperature and high-temperature layers can be described by the same apparent diffusivity. Incidentally, this also suggests that the porosity of the pre-oxidized layer (assessed from SEM images to be approximately 5 %, primarily due to cracks between sublayers and still present after high-temperature oxidation [7,64]) has minimal or no influence on oxygen transport. This aligns with data obtained at 850 °C using ^{18}O as a diffusion tracer, which indicated limited oxygen ingress through the porosities of the pre-oxidized layer [64]. Conversely, at 1100 °C, experimental TGA curves lie notably below the calculated ones, indicating that the passivation effect of the low-temperature pre-oxidized layer is much stronger than that of a high-temperature scale. This could be attributed to the fact that the pre-oxidized layer remains predominantly monoclinic at 1100 °C and transforms into the tetragonal phase when heated to 1200 °C. This is

consistent with the Zr-O phase diagram, which indicates a monoclinic to tetragonal phase transformation at 1205 °C [55]. At 900 °C and 1000 °C, although curves calculated from Eq. (3) have not been plotted, it is evident that the protective influence of the pre-oxidized layers remains strong.

Therefore, for the purposes of modeling LOCA oxidation and as a simplified approach, it is suggested that the effect of pre-oxidation could be calculated considering 1200 °C as a threshold, below which oxygen diffusion through the pre-oxidized scale is simulated using monoclinic zirconia diffusivity values and above which tetragonal zirconia diffusivity is preferred.

5. Conclusion

A modified thermobalance was employed for steam oxidation tests in the temperature range of 900–1200 °C for three alloys: Zircaloy-4, $M5_{Framatome}$, and Optimized ZIRLO, using both as-received tubes and pre-oxidized specimens. For the as-received specimens, significant differences in oxidation rates were observed among the three alloys in the lower temperature range (up to 1000 °C), with M5 exhibiting a more favorable behavior. At 1000 °C, as the breakaway transition was approached, a notable deceleration of kinetics was noted for Zy4 and Optimized ZIRLO, attributed to the formation of porosities at the metal/oxide interface, which may precede the transition. Conversely, no breakaway transition was observed for M5 over extended durations. Beyond the breakaway transition regime, at 1100 °C and above, the alloy composition appeared to have no discernible influence on the oxidation rate, with kinetic curves converging for all three alloys.

With pre-oxidized specimens, the protective effect against high-temperature oxidation of a zirconia layer formed at low temperature was confirmed. Initially, due to the stoichiometry of the zirconia, it was expected that the pre-oxidized layer would be non-conductive, and a period of zero mass gain rate was anticipated at the beginning of steam exposure. However, oxygen uptake was observed to commence immediately, suggesting that a gradient of oxygen vacancies rapidly establishes across the pre-oxidized layer. Although the underlying physics require further investigation, the protective properties of the pre-oxidized layer are effective, resulting in a significantly lower mass gain rate compared to bare claddings up to 1100 °C. At 1200 °C, the protective effect weakens, likely due to the monoclinic to tetragonal zirconia transformation.

CRediT authorship contribution statement

C. Duriez: Writing – original draft, Validation, Methodology, Investigation, Formal analysis, Data curation, Conceptualization. **H. Richez:** Methodology, Investigation. **C. Eymery:** Methodology, Investigation. **J. Desquines:** Writing – review & editing. **S. Guilbert:** Writing – review & editing, Validation, Formal analysis, Data curation.

Declaration of competing interest

The authors declare that they have no known competing financial interests or personal relationships that could have appeared to influence the work reported in this paper.

Data availability

Data will be made available on request.

Supplementary materials

Supplementary material associated with this article can be found, in the online version, at doi:10.1016/j.jnucmat.2024.155147.

References

[1] United States Department Of Energy, New acceptance criteria for emergency core-cooling systems of light-water-cooled nuclear power reactors, Nucl. Safety 15 (1974) 173–184.

[2] G. Hache and H.M. Chung, "The History of LOCA Embrittlement Criteria," Report NUREG/CP-0172, pp. 205–237, 2001.

[3] S. Leistikow, G. Schanz, and H.V. Berg, "Kinetik und Morphologie der isothermen Dampf-Oxidation von Zircaloy 4 bei 700-1300°C " Report KFK 2587, Germany, 1978.

[4] V. Vrtilkova, "Review of Recent work at UJP PRAHA on the LOCA Embrittlement Criterion," in 6th Plenary Meeting of the OECD/CSNI/SEGFSM, Paris, France, 2005.

[5] M.Le Saux, J.C. Brachet, V. Vandenberghe, E. Rouesne, S. Urvoy, A. Ambard, R. Chosson, Effect of a pre-oxide on the high temperature steam oxidation of Zircaloy-4 and M5Framatome alloys, J. Nucl. Mater. 518 (2019) 386–399.

[6] M.Le Saux, J.C. Brachet, V. Vandenberghe, D. Gilbon, J.P. Mardon, B. Sebbari, Influence of pre-transient oxide on LOCA high temperature steam oxidation and post-quench mechanical properties of Zircaloy-4 and M5™ cladding, in: LWR Fuel Performance Meeting/top Fuel/WRFPM 2011, Chengdu, China, 2011.

[7] S. Guilbert-Banti, A. Viretto, J. Desquines, C. Duriez, Effect of pre-oxide on Zircaloy-4 high temperature steam oxidation, J. Nucl. Mater. 548 (2021) 152857.

[8] S. Guilbert, P. Lacote, G. Montigny, C. Duriez, J. Desquines, C. Grandjean, Effect of pre-oxide on Zircaloy-4 high temperature steam oxidation and post-quench mechanical properties, in: R. Comstock, P. Barbéris (Eds.), Zirconium in Nuclear Industry: 17thInternational Symposium, ASTM STP 1543, ASTM International, West Conshohocken, PA, USA, 2014, pp. 1–27.

[9] M. Ozawa, T. Takahashi, T. Homma, K. Goto, Behavior of Irradiated Zircaloy-4 Fuel Cladding under Simulated LOCA Conditions, in: Zirconium in the Nuclear Industry: 12thInternational Symposium, ASTM STP 1354, Toronto, Canada, 2000, pp. 279–299.

[10] F. Nagase, T. Otomo, M. Tanimoto, H. Uetsuka, Experiments on high Burnup fuel Behavior Under LOCA Conditions at JAERI, in: Light Water Reactor Fuel Performance, Park City, Utah, USA, 2000.

[11] T. Fuketa, JAERI Experimental Basis on RIA and LOCA, in: OECD/CSNI/SEGFSM meeting, Paris, France, 2005.

[12] T. Chuto, Oxidation of High Burnup Fuel Cladding in LOCA Conditions, in: Fuel Safety Research Meeting, Tokai, Japan, 2010.

[13] J.T. Prater and E.L. Courtright, "Oxidation of Zircaloy-4 in Steam at 1300 to 2400°C," R. B. Adamson and L. Van, Eds., ed West Conshohocken, PA, USA: ASTM International, 1987, pp. 489–501.

[14] S. Leistikow, S.G. Schanz, The oxidation behavior of Zircaloy-4 in steam between 600 and 1600°C, Mater. Corros. 36 (1985) 105–116.

[15] J.C. Brachet, L. Portier, T. Forgeron, J. Hivroz, D. Hamon, T. Guilbert, T. Bredel, P. Yvon, J.P. Mardon, and P. Jacques, "Influence of Hydrogen content on the α/β phase Transformation and on the Thermal-mechanical Behavior of Zy-4, M4 and M5 Alloys During the First Phase of LOCA transient," in Zirconium in the Nuclear Industry: 13th International Symposium, ASTM-STP 1423, Annecy, France, 2001, pp. 673–701.

[16] C. Duriez, S. Guilbert, A. Stern, C. Grandjean, L. Belovský, J. Desquines, Characterization of oxygen distribution in LOCA situations, J. ASTM. Int. 8 (2011).

[17] L. Yegorova, K. Lioutov, N. Jouravkova, A. Konobeev and V.C.V. Smirnov, A. Goryachev, "Experimental Study of Embrittlement of Zr-1%Nb VVER Cladding under LOCA-Relevant Conditions," International Agreement Report NUREG/IA-02111, IRSN 2005-194, NSI RRC KI 3188, 2005.

[18] C. Duriez, T. Dupont, B. Schmet, F. Enoch, Zircaloy-4 and M5 High Temperature Oxidation and Nitriding in air, J. Nucl. Mater. 380 (2008) 30–45.

[19] M. Lasserre, V. Peres, M. Pijolat, O. Coindreau, C. Duriez, J.P. Mardon, Modelling of Zircaloy-4 accelerated degradation kinetics in nitrogen-oxygen mixtures at 850°C, J. Nucl. Mater. 462 (2015) 221–229.

[20] M. Gestin, M. Mermoux, O. Coindreau, C. Duriez, M. Pijolat, V. Peres, L. Favergeon, Experimental study of oxidation in oxygen, nitrogen and steam mixtures at 850∘C of pre-oxidized Zircaloy-4, J. Nucl. Mater. 519 (2019) 302–314.

[21] M. Steinbrück, Prototypical Experiments Relating to air Oxidation of Zircaloy-4 at high Temperatures, J. Nucl. Mater. 392 (2009) 531–534.

[22] Y. Nemoto, Y. Kaji, C. Ogawa, K. Nakashima, M. Tojo, Influence of the Air/Steam Mixing Ratio in Atmosphere on Zirconium Cladding Oxidation in Spent Fuel Pool Accident Condition, in: Water Reactor Fuel Performance Meeting, Jeju Island, Korea, 2017.

[23] J.L. Vandegrift, P.M. Price, J.-P. Stroud, C.J. Parga, I.J. Van Rooyen, B.J. Jaques, D. P. Butt, Oxidation behavior of Zirconium, Zircaloy-3, Zircaloy-4, Zr-1Nb, and Zr-2.5Nb in air and oxygen, Nucl. Mater. Energy 20 (2019) 100692. /08/01/2019.

[24] M. Suzuki, S. Kawasaki, and T. Furuta, "*Zircaloy Steam Reaction and Embrittlement of the Oxidized Zircaloy tube under postulated Loss of Coolant Accident Conditions*," US-NRC Report NUREG-TR-0014, USA, 1977.

[25] J.H. Baek, K.B. Park, Y.H. Jeong, Oxidation kinetics of Zircaloy-4 and Zr–1Nb–1Sn–0.1Fe at temperatures of 700–1200°C, J. Nucl. Mater. 335 (2004) 443–456.

[26] J.H. Baek, Y.H. Jeong, Steam Oxidation of Zr-1.5Nb-0.4Sn-0.2Fe-0.1Cr and Zircaloy-4 at 900-1200°C, J. Nucl. Mater. 361 (2007) 30–40.

[27] J.H. Baek, Y.H. Jeong, Breakaway Phenomenon of Zr-based Alloys During a high-Temperature Oxidation, J. Nucl. Mater. 372 (2008) 152–159.

[28] M. Steinbrück, N. Vér, M. Grosse, Oxidation of advanced zirconium cladding alloys in steam at temperatures in the range of 600-1200°C, Oxidation Metals 76 (2011) 215–232.

[29] R. Zino, R. Chosson, M. Ollivier, E. Serris, L. Favergeon, Parallel mechanism of growth of the oxide and α-Zr(O) layers on Zircaloy-4 oxidized in steam at high temperatures, Corros. Sci. 179 (2021) 109178.
[30] M.C. Collins, G.J. Francolini, P. Obreja, N. Scuro, R. Varga, B. Breeden, D. Rosas, B. W.N. Fitzpatrick, E. Geiger, G. Harvel, M.H.A. Piro, A comparison of thermo-oxidation kinetic measurements of Zircaloy-4 in light and heavy water steam, J. Nucl. Mater. 573 (2023) 154111.
[31] H.H. Kim, J.H. Kim, J.Y. Moon, H.S. Lee, J.J. Kim, Y.S. Chai, High-temperature Oxidation Behavior of Zircaloy-4 and ZIRLO in Steam Ambient, J. Mater. Sci. Technol. 26 (2010) 827–832, 2010/01/01/.
[32] C. Duriez, O. Coindreau, M. Gestin, A. Kasperski, V. Peres, M. Pijolat, H. Buscail, C. Issartel, R. Rolland, M. Mermoux, Zircaloy-4 high temperature oxidation in atmospheres representative of SFP-LOCA: investigation of the influence of a low temperature pre-oxidation scale, J. Nucl. Mater. 513 (2019) 152–174.
[33] J.P. Mardon, B. Dunn, Overview of the M5 Alloy Behavior under RIA and LOCA Conditions, in: 2007 International Meeting on the LWR Fuel Performance, San Franscico, California, 2007.
[34] United State - Nuclear Regulatory Commission (US-NRC), "*Regulatory Guide 1.222 - Measuring Breakaway Oxidation Behavior*," Report ML15281A170, USA, 2015.
[35] T. Furuta, S. Kawasaki, Reaction Behavior of Zircaloy-4 in Steam-Hydrogen Mixtures at High Temperature, J. Nucl. Mater. 105 (1982) 119–131.
[36] R. Zino, Modélisation cinétique de l'oxydation des alliages de zirconium à haute température sous vapeur d'eau et approfondissement des mécanismes du breakaway, PhD Thesis, École des Mines de Saint-Étienne, St Etienne, France, 2021.
[37] Z. Hózer, C. Gyori, L. Matus, M. Horváth, Ductile-to-Brittle Transition of Oxidised Zircaloy-4 and E110 Claddings, J. Nucl. Mater. 373 (2008) 415–423.
[38] J.C. Brachet, V. Vandenberghe-Maillot, L. Portier, D. Gilbon, A. Lesbros, N. Waeckel, J.-P. Mardon, Hydrogen Content, Preoxidation, and Cooling Scenario Effects on Post-Quench Microstructure and Mechanical Properties of Zircaloy-4 and M5 Alloys in LOCA conditions, in: B. Kammenzind, M. Limbäck (Eds.), Zirconium in Nuclear Industry: 15thInternational Symposium, ASTM STP 1505, 5, ASTM International, ed Sunriver, Oregon, 2008, pp. 91–118.
[39] S. Guilbert, C. Duriez, C. Grandjean, Influence of a Pre-Oxide Layer on Oxygen Diffusion and on Post-Quench Mechanical Properties of Zircaloy-4 After Steam Oxidation at 900°C, in: LWR Fuel Performance Meeting/top Fuel/WRFPM 2010, Orlando, Florida, USA, 2010.
[40] J.V. Cathcart, R.E. Pawel, R.A. McKee, R.E. Druschel, G.J. Yurek, J.J. Campbell, and S.H. Jury, "*Zirconium Metal-Water Oxidation Kinetics IV. Reaction rate Studies*," Report ORNL/NUREG-17, USA, 1977.
[41] T. Chuto, F. Nagase, T. Fuketa, High Temperature Oxidation of Nb-Containing Zr Alloy Cladding in LOCA Conditions, Nucl. Eng. Technol. 41 (2009) 163–170.
[42] M. Billone, Y. Yan, T. Burtseva, and R. Daum, "*Cladding Embrittlement During Postulated Loss-of-Coolant Accidents*," United States-Nuclear Regulatory Commission Report NUREG-CR-6967, USA, 2008.
[43] R.E. Pawel, J.V. Cathcart, R.A. McKee, The Kinetics of Oxidation of Zircaloy-4 in Steam at high Temperatures, J. Electrochem. Soc. 126 (1979) 1105–1111.
[44] F. Nagase, T. Otomo, H. Uetsuka, Oxidation kinetics of low-Sn Zircaloy-4 at the temperature range from 773 to 1,573 K, J. Nucl. Sci. Technol. 40 (2003) 213–219.
[45] C.M. Lee, Y.-K. Mok, D.-S. Sohn, High-temperature steam oxidation and oxide crack effects of Zr-1Nb-1Sn-0.1Fe fuel cladding, J. Nucl. Mater. 496 (2017) 343–352.
[46] C. Wagner, Beitrag zur theorie des anlaufvorgangs, Z. phys. Chem. 21 (1933) 25.
[47] H. Uetsuka, P. Hofmann, High-temperature oxidation kinetics of Zircaloy-4 in oxygen/argon mixtures, J. Nucl. Mater. 168 (1989) 47–57.
[48] M. Guerain, C. Duriez, J.L. Grosseau-Poussard, M. Mermoux, Review of stress fields in Zirconium alloys corrosion scales, Corros. Sci. 95 (2015) 11–21.
[49] C. Valot, "*Techniques de diffraction RX et dynamique spatio-temporelle de l'oxydation des métaux des groupes 4 et 5: application au Zirconium*," Thesis, Université de Bourgogne, France, 1995.
[50] I. Idarraga, M. Mermoux, C. Duriez, A. Crisci, J.P. Mardon, Potentialities of Raman Imaging for the Analysis of Oxide Scales Formed on Zircaloy-4 and M5 in Air at High Temperature, Oxidat. Metals 79 (2013) 289–302.
[51] P. Bouvier, "*Etude Raman des distributions de phases et de contraintes dans des couches d'oxydation d'alliages de zirconium*," PhD Thesis, Institut National Polytechnique de Grenoble, France, 2000.
[52] J. Godlewski, P. Bouvier, G. Lucazeau, L. Fayette, Stress Distribution Measured by Raman Spectroscopy in Zirconia Films Formed by Oxidation of Zr-Based Alloys, in: G.P. Sabol, G.D. Moan (Eds.), Zirconium in the Nuclear Industry: 12thInternational Symposium, ASTM STP 1354, ed ASTM International, West Conshohocken, PA, 2000, pp. 877–900.
[53] I. Idarraga, Etude des mécanismes de dégradation sous air à haute température des gaines de combustible nucléaire en alliage de zirconium, Université de Grenoble, France (2011).
[54] P. Bouvier, J. Godlewski, G. Lucazeau, A Raman Study of the Nanocrystallite size Effect on the Pressure-Temperature Phase Diagram of Zirconia Grown by Zirconium-Based Alloys Oxidation, J. Nucl. Mater. 300 (2002) 118–126.
[55] J.P. Abriata, J. Garcés, R. Versaci, The O-Zr (Oxygen-Zirconium) System, Bull. Alloy Phase Diagrams 7 (1986) 116–124.
[56] S. Shukla, S. Seal, Mechanisms of room temperature metastable tetragonal phase stabilisation in zirconia, Int. Mater. Rev. 50 (2005) 45–64.
[57] D. Gosset, M. Le Saux, In-situ X-ray diffraction analysis of zirconia layer formed on zirconium alloys oxidized at high temperature, J. Nucl. Mater. 458 (2015) 245–252.
[58] R. Guillou, M. Le Saux, E. Rouesne, D. Hamon, C. Toffolon-Masclet, D. Menut, J. C. Brachet, J.L. Béchade, D. Thiaudière, In-situ time-resolved study of structural evolutions in a zirconium alloy during high temperature oxidation and cooling, Mater. Charact. 158 (2019) 109971.
[59] R. Zino, R. Chosson, M. Ollivier, E. Serris, Breakaway characterization of Zircaloy-4 oxidized in steam and in oxygen at high temperatures using HT- XRD analysis, Corros. Sci. 176 (2020) 109028.
[60] J. Debuigne, P. Lehr, Étude de l'oxydation du zirconium non allié et de la diffusion de l'oxygène dans la couche d'oxyde et dans le métal, Mem. Sci. Rev. Metallurg. 60 (1963) 911.
[61] A. Denis, E.A. Garcia, Diffusion in a semi-Infinite System with a Moving Interphase Considering Solvent Density Change: application to the Oxidation of Zirconium, J. Nucl. Mater. 96 (1981) 127–140.
[62] K. Park, D.R. Olander, Oxygen Diffusion in Single-Crystal Tetragonal Zirconia, J. Electrochem. Soc. 138 (1991) 1154–1159.
[63] X. Ma, C. Toffolon-Masclet, T. Guilbert, D. Hamon, J.C. Brachet, Oxidation Kinetics and Oxygen Diffusion in low-tin Zircaloy-4 up to 1523 K, J. Nucl. Mater. 377 (2008) 359–369.
[64] A. Kasperski, C. Duriez, M. Mermoux, Combined Raman imaging and ^{18}O tracer analysis for the study of Zircaloy-4 high temperature oxidation in spent fuel pool accident, in: R.J. Comstock, A.T. Motta (Eds.), Zirconium in Nuclear Industry: 18thInternational Symposium, ASTM STP1597, ASTM international, West Conshohocken, PA, 2018, pp. 1059–1092.